International Journal of Modern Manufacturing Technologies
ISSN 2067–3604, Vol. XVI, No. 3 / 2024
https://doi.org/ 10.54684/ijmmt.2024.16.3.122

INVESTIGATING THE INFLUENCE OF INFILL DENSITY AND POST-PROCESSING PARAMETERS ON 3D PRINTED PLA COPPER COMPOSITE

Mohamad Nor Hafiz Jamil[1], Ahmad Zahirani Ahmad Azhar[1], Nor Aiman Sukindar[1,2], Ahmad Shah Hizam Md Yasir[3], Sharifah Imihezri Syed Shaharuddin[1], Wan Mohd Fazli Wan Nawawi[1], Mohamad Talhah Al Hafiz[1]

[1]International Islamic University Malaysia, Department of Manufacturing and Material
53100 Gombak, Selangor, Malaysia
[2]School of Design, Universiti Teknologi Brunei, Tungku Highway, Gadong BE1410, Brunei Darussalam
[3]Faculty of Resilience Rabdan Academy, 65, Al Inshirah, Al Sa'adah, Abu Dhabi
22401, PO Box: 114646, Abu Dhabi, UAE

Corresponding author: Nor Aiman Sukindar, noraimansukindar@gmail.com

***Abstract*:** Fused deposition modelling (FDM) is a common 3D printing technique currently in use. FDM can now produce metal products using a cost-effective technology developed by the Virtual Foundry filament. Analyze various parameters, and this study investigated the effects of three parameters: infill density, holding hours of debinding, and sintering. Each parameter was tested at different levels using a copper metal filament composite, including shrinkage and porosity. Nine print runs were conducted by changing three parameters using the Taguchi method. The analysis found that the composition of all samples was almost the same, regardless of the different parameters and settings. The density of the infill has a significant impact on shrinkage. To prevent significant shrinkage during post-processing, the ideal infill density is 100%. In conclusion, the parameters do not affect the material composition. The infill density is a printing parameter proven to be more important than post-processing parameters, holding hours for debinding and sintering in terms of dimensional accuracy, shrinkage, and porosity.
Key words: Fused deposition modelling, Copper-PLA, Debinding, Sintering, Infill density

1. INTRODUCTION

Additive Manufacturing (AM) technologies have had a substantial impact on industries such as medical, aerospace, automotive, food, and engineering due to their broad use, providing several benefits and revolutionising different sectors, [1]. 3D printing is increasingly utilised notably in dentistry and orthodontics. The ability to digitally acquire, modify, and replicate dental arches has significantly revolutionised operations in the industry, [2]. Orthopaedics has several opportunities for additive manufacturing (AM) to revolutionise procedures. The lack of a suitable lubricating material hinders the realisation of these possibilities, [3].
There are several types (processes) of 3D printing that common choices. Stereolithography (SLA) is among the choices. This technique creates three-dimensional objects by solidifying liquid resin selectively using a photopolymerization reaction. [4] Fused Deposition Modelling (FDM) is one the another with a diverse 3D printing technology that uses plastic or polymer-based materials like ABS and PLA. This technology is versatile and can be used in several industries for purposes such as prototyping, manufacturing, and quick production, [5]. Researchers discovered and conducted experiments to analyse the effects of different mechanical responses, such as bending, stress, and torsion, on 3D-printed materials made utilising Fused Deposition Modelling (FDM) technology with diverse composite material filaments, [6]. Virtual Foundry, a prominent filament brand, made a huge breakthrough in 3D printing in 2015 with the introduction of a metal infill filament. This breakthrough revolutionised the industry by enabling the incorporation of metal characteristics into printed objects using Fused Deposition Modelling (FDM). This was a significant advancement in metal fabrication, creating new possibilities for fabricating metal components through additive manufacturing methods, [7].
3D printing technology, particularly in Fused Deposition Modelling (FDM), has made significant progress. Shenzhen Tuozhu Technology Co. Ltd., the parent company of Bambu Labs, introduced high-speed printers that can achieve speeds between 300mm/s and 500mm/s. This innovation has led to advancements in the industry, pushing manufacturers to improve their systems to match the higher printing rates and fulfil the increasing

requirements for efficiency and productivity, [8]. The advancement materials of filament available helps to push forwards the FDM technology. Fused Deposition Modelling (FDM) is a modern technique used to create green bodies for sintering, in contrast to Metal Injection Moulding (MIM). FFF uses filament feedstock material, which results in lower installation costs and allows for a wide range of geometries without the necessity of costly mould design, unlike MIM's granule-based feedstock, [9].

Now, there also a specialised machine was created with financial support from the European Space Agency (ESA), incorporating both a debinding heater and a sintering heater. The hybrid machine includes a low-intensity infrared diode laser and an induction heater. The machine is a Fused Deposition Modelling (FDM) device that can conduct localised debinding and sintering processes right after the printing phase, [10]. This prototype machine helps to reduce the time to prepare sample for debinding and sintering process.

In term of cost, printing the design using Fused Deposition Modelling (FDM) was EUR 246.13, whereas it was EUR 1147.88 for Selective Laser Melting (SLM). The cost specifically refers to the green element in the FFF scenario. It is crucial to factor in the cost of sintering, which usually averages about 60 EUR/kg. Even after considering the cost of sintering, the final price is far cheaper than the projected cost for Selective Laser Melting (SLM), [11]. The qualities of materials produced through 3D printing are greatly influenced by the specific processing settings used, considering the automated nature of the process itself. The infill density is vital in influencing the deformation and strength characteristics of the material, while also contributing to cost reduction, [12]. Despite being a recent breakthrough, there are still some unknown features of the debinding and sintering method applied for samples from Fused Deposition Modelling (FDM). This study intends to examine how infill density, debinding holding hours, and sintering affect material composition, z-axis dimensions, and porosity, providing insight into key factors for improving the FFF process.

Parameters of printing during the slicing effected the results of product produce. When printing PLA-Aluminum composite materials, the Ra value, indicating surface roughness, is notably affected by both layer thickness and raster angle. The most relevant parameter is layer thickness, with raster angle following closely behind. Printing speed does not have a substantial impact on surface roughness according to these data, [13].

The correlation between printing parameters and post-processing parameters differs greatly throughout several publications that concentrate on creating sintered objects through Fused Deposition Modelling (FDM). The variations emphasise the range of techniques and strategies used in the field. Several articles demonstrate various settings for producing sintered parts using FFF technology, highlighting its versatility and adaptability in manufacturing. This author, make a preparation involved using filament bronze from Virtual Foundry, and tensile testing was conducted following ASTM standards. The sample preparation for debinding and sintering involved using Magic Black Powder (MBP) mixed with a small amount of water to get the desired consistency that was neither too runny nor too sticky. Initial experiments were carried out on infill densities of 20, 50, and 100, with 100 being chosen to avoid brittleness. The sintering peak temperature was regulated. Energy Dispersive X-ray Spectroscopy (EDS) analysis indicated that the composition of the printed objects was not affected by the sintering temperature, [14]. The article employed an alternative way following the manufacturer's guidelines to prepare the sample prior to proceed the debinding and sintering procedure. The author successfully sintered the samples to perfection, maintaining their good state.

Next, this author utilised materials are Ultrafuse 316L from BASF, including 90% of 316L stainless steel and 10% polyoxymethylene (POM). Factors including nozzle temperature, nozzle diameter, and extrusion speed are essential for the processes. Nitric acid is used in catalytic debinding to dissolve the POM primary binder matrix. It is crucial to monitor and reduce the impact of the spring preload of the drive gears on the actual material feed. Furthermore, it is important to meticulously regulate the nozzle temperature to prevent it from beyond specific thresholds when processing. Increased temperatures lower viscosity and back pressure in the nozzle but can also cause thermal deterioration. This deterioration not only results in a decrease in mass but can also present health risks. Thus, it is crucial to uphold ideal processing conditions to guarantee the quality and safety of the printed components, [15]. The study uses the cataylic debinding method to dissolve the binder from the sample. Which is different from this experiment and the guideline of Virtual Foundry.

In this paper, the author uses Zetamix YSZ white zirconia filament, which contains 50% YSZ powder, was processed using a special method. The filament was first chemically debound in acetone, eliminating around half of the binder. The material was subjected to thermal debinding and densification using ultrafast high-temperature sintering (UHS) in a single-step procedure that lasted (30–120) seconds. The sintered products produced were found to be free of cracks, even under microscopic scrutiny, showcasing the efficiency of this novel processing technique, [16]. This author employed a fascinating technique for sintering. Ultrafast high-temperature sintering is a rapid process. However, it requires costly equipment in comparison to a furnace.

As for this article, the filament utilised was composed of 60% by volume of 316L stainless steel particles with an average diameter of 10 μm, and 40% by volume of an organic binder sourced from Taisei Kogyo Co. Ltd., Osaka,

Japan. Factors like layer thickness and printing orientation were considered during the printing procedure. The thermal debinding and sintering procedures were place in a single vacuum furnace. The linear shrinkage in the layer direction ranged from 15% to 17%, whereas in the perpendicular directions it ranged from 14% to 15%. The specimen printed with the layer direction perpendicular to the tensile direction had the maximum ultimate strength of 453 MPa and a strain at break of 48%. Emphasising the significance of printing orientation in obtaining the intended mechanical qualities in the product, [17].

The study examined BASF's commercial metal-polymer filament, Ultrafuse 316L, by investigating factors such nozzle temperature, layer thickness, and flow rate. Increasing the flow rate from 100% to 110% considerably improved all mechanical properties, sample density, and decreased porosity and average particle size, making it the most crucial factor. Enhancing layer thickness from 90 to 140 μm enhanced mechanical performance and reduced average grain size, without changing flow rate and nozzle temperature. A reduction in nozzle temperature from 250°C to 240°C improved the tensile and bending characteristics of the printed specimens. These findings highlight the necessity of precisely adjusting printing conditions to attain the desired material characteristics and performance in metal-polymer filament printing, [18].

The sample was made of bronze and had the shape of a cube with 10mm dimensions. The orientation of sintering was controlled by placing the sample between sand in the crucible during the process. The different sintering orientations showed minimal impact on shrinkage and porosity. Results from various sintering orientations produced comparable results. The shrinkage in the z-axis direction was less than in the x and y directions, impacting the shrinkage and density of the sintered parts. The porosity formed during printing had a direct impact on the dimensional shrinkage of the product, [19].

The goal is to develop low-cost metal products by adjusting infill density and optimising the timing of debinding and sintering procedures. The project intends to examine how changing infill density and the duration of debinding and sintering affect material composition. The research will assess the accuracy of dimensions on the z-axis as well as mass loss related to dimension accuracy. The finished product's porosity will be evaluated to guarantee the best quality and functionality.

2. MATERIALS AND METHODS

2.1. Materials

The study used Copper Filament™, a metal filament produced by The Virtual Foundry Company (Stoughton, WI, 53589, United States), specifically tailored for 3D printing purposes. The filament is composed of 85% copper powder, 15% polylactic acid (PLA), and a binder. This innovative blend improves the heat-conducting abilities of copper and takes advantage of the user-friendly nature of PLA.

2.2. 3D Printer Setup and Sample Design

The study selected the Sidewinder version X2 3D printer manufactured by Artillery3D (China) because of its direct drive technology, which allows for perfect filament extraction directly to the extruder. A 0.8mm hardened steel nozzle was used to increase the flow rate while printing. The 30mm cubic sample refer figure 1 was created using SolidWorks 2021 by Dassault Systemes and converted to Stereolithography (STL) format. The design was converted into printed instructions using slicer software, Cura version 5.0 by Ultimaker, which supports STL format.

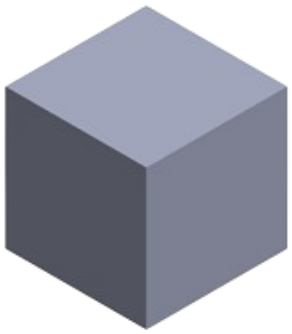

Fig. 1. Cube sample design from SolidWorks 2021

The printer settings were designed to align with the investigation's objectives, guaranteeing the best printing circumstances. Many of the parameters are still configured with their default values as recommended by Cura. However, specific changes need to be implemented. Table 1 illustrates the parameters that change.

Table 1. List of setup parameters in Cura software.

Parameter	Value	Unit
Printing Speed	20	mm/s
Infill Density	20-100	%
Infill Pattern	Lines	-

2.3. Debinding and Sintering Process

This instruction was modification from the manufacturer. Both the sintering and debinding processes in this investigation employed heat methods. The porcelain crucible, with a volume of 300ml, was filled with Al_2O_3 powder, leaving about 20mm of room at the bottom. The green sample was positioned in the centre and covered with Al_2O_3 powder until it reached a height of 20mm from the top, then the crucible was sealed with a lid. The crucible was then placed in the furnace and the temperature was raised progressively by 5°C per minute until it reached 482°C. The sample was kept at a specific temperature for different durations between 1 and 7 hours to identify the best holding time for the debinding process. After the designated holding period, the crucible was cooled inside the furnace until it reached room temperature, and then the sample was taken out for additional analysis.

The crucible is filled with Magnesium Silicate refractory for the sintering process, leaving around 20mm of space from the bottom initially. The brown sample is then precisely placed in the middle of the crucible. The area surrounding the sample is filled with Magnesium Silicate refractory, leaving about 25mm of room at the top. The remaining space in the crucible is filled with sintering carbon until it is completely full, and then the crucible is sealed with a lid. The crucible is placed in the furnace and heated at a pace of 10°C per minute until it reaches a temperature of 1052°C. The sample is maintained at 1052°C for different durations between 2 to 8 hours after reaching the target temperature, with the aim of identifying the most effective holding time for the sintering process. After the designated holding period, the crucible is cooled within the furnace until it reaches room temperature. The sample is then taken out, marking the end of the sintering process.

2.4. DOE Using Taguchi Method

This study will investigate three parameters using the Taguchi method generated by Minitab version 18 software by Triola Statistics Company, due to their suitability. Each factor contains three levels, as detailed in the table 2 below:

Table 2. DOE Taguchi Method

No.	Infill Density (%)	Holding Hours for Debinding (hour)	Holding Hours for Sintering (hour)
1	100	7	8
2	100	4	5
3	100	1	2
4	60	7	5
5	60	4	2
6	60	1	8
7	20	7	2
8	20	4	8
9	20	1	5

2.5. Shrinkage Analysis

The z-axis and xy dimensions of the samples were measured using a digital vernier calliper before and after the sintering process. The samples' shrinkage was computed and documented using these measures.

2.6. Porosity Analysis

The samples were examined under a microscope, with observations conducted at four distinct locations on the surface to guarantee a thorough study. The microscope used was model BX41M manufactured by Olympus (Tokyo, Japan). The software used to calculate porosity from microscopic observations is Stream Basic from Olympus. It enables precise quantification and study of porosity in the materials.

2.7. EDX Analysis

The metal samples undergo analysis with a scanning electron microscope (SEM), specifically the JSM-IT100 model produced by Jeol (Mitaka, Tokyo, Japan). This study is being undertaken to identify the material composition of the samples. Additionally, energy-dispersive X-ray spectroscopy (EDX) analysis is conducted post-sintering to provide further characterization of the materials.

3. RESULTS AND DISCUSSION

The early examples produced using the default configurations of the 3D printer recommended by the slicer software, Cura version 5.0, exhibited evident imperfections. Figure 2 displays a noticeable defect, marked by the division of layers and uneven material distribution. This flaw is most evident in the cube's side section. Visual inspections confirmed that the samples had brittleness, indicating insufficient mechanical properties. The flaws discovered in the sample printed using the default settings emphasize the limitations of using pre-established parameters for producing delicate copper composite filament. Although these settings are typically enough for regular materials, they usually do not consider the precise flow rate, heat conditions, and extrusion requirements necessary to create the best possible layer adhesion in copper composite materials. Figures 3 and 4 show that the layers don't stick together well enough, which causes the structure to be weak. This means that the printing settings aren't right for the unique properties of copper composite filaments.

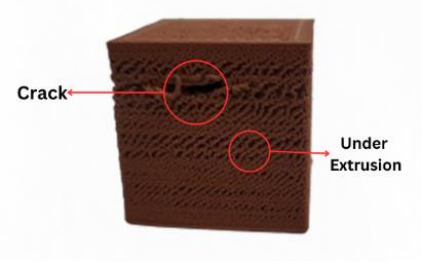

Fig. 2. Defect sample

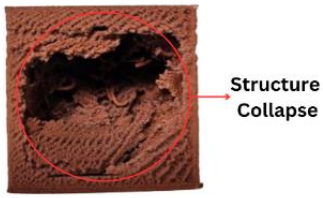

Fig. 3. Structure problem

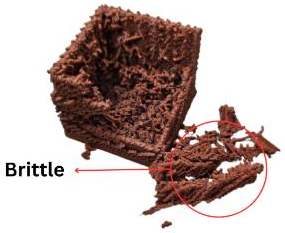

Fig. 4. Brittle sample

Under extrusion in FDM printing occurs when the printer cannot supply the necessary amount of filament to form a solid, continuous line, resulting in weak and incomplete prints. This issue can be particularly pronounced when using high-percentage copper composite filaments due to their unique properties. The flow rate is critical in determining the success of printing with copper composite filaments. At a high print speed of 60 mm/s, the printer may not be able to maintain a consistent extrusion rate, leading to under extrusion. This results in gaps, weak layer adhesion, and an overall reduction in the structural integrity of the printed part.

Research indicates that reducing the print speed significantly improves the print quality of copper composite filaments. This adjustment allows the extruder to keep up with the required material output, ensuring a more consistent and robust deposition of the filament. Studies focusing on the mechanical properties and surface quality of metal composites in FDM processes corroborate this,[20].

Nevertheless, a single study demonstrated that utilising a copper composite filament and printing at a speed of 60 mm/s resulted in the production of high-quality samples. The copper composite filament in this study consisted of around 20% to 40% copper, [21]. Printing at a speed of 60mm/s using the default setting is only practicable for filaments that have a copper content of up to 40%.

The printed cube in Figure 5 illustrates how changing the crucial parameter, specifically the printing speed, from the default 60 mm/s to 20 mm/s, improved the sample's structural integrity and surface smoothness. This sample exhibited no indications of the flaws previously observed at greater velocities, such as delamination or material irregularity. The reduced printing speed enhanced layer adhesion and enabled more accurate material deposition, leading to a consistently structured and visually appealing surface.

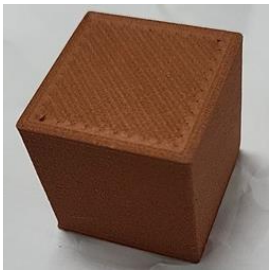

Fig. 5. Sample printed using 20mm/s

Figure 6 presents the raw data from samples tested for shrinkage along the Z-axis. This data is critical for understanding how the material behaves under certain circumstances. Significantly, whereas most samples displayed the anticipated reduction in size, the data indicates that one sample had an increase in size instead of a decrease. This abnormality necessitates further analysis to understand the fundamental origins and ramifications for the material's performance and dependability.

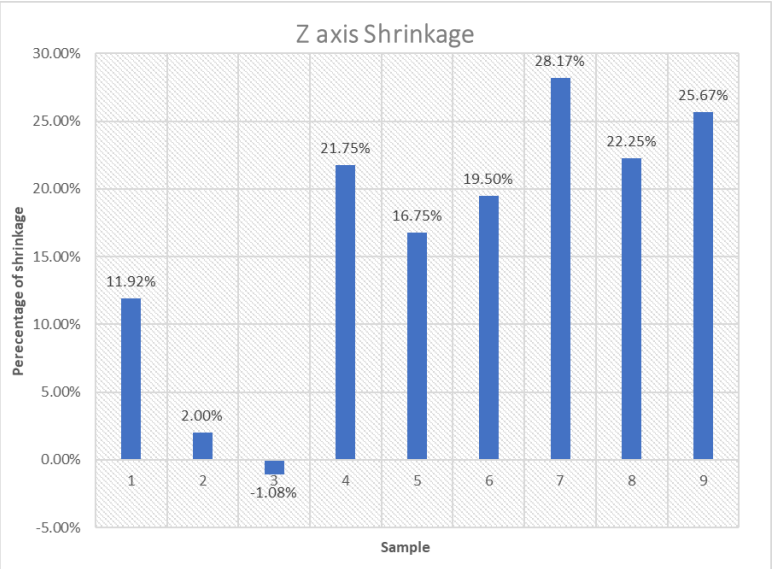

Fig. 6. Graph of z axis shrinkage

My theory about the observed expansion in Sample 3 is that the process did not allow the copper atoms to fully sinter. This is likely due to the brief holding period during the sintering stage. Sample 3 is using a 100% infill density setting. This demonstrates that a brief period of debinding and sintering for a 100% sample will result in its expansion. Figures 7, 8, and 9 show the SEM analysis between the 100% infill density sample, which is sample 1, sample 2, and sample 3.

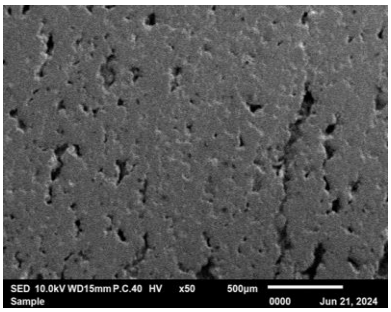

Fig. 7. sample 1

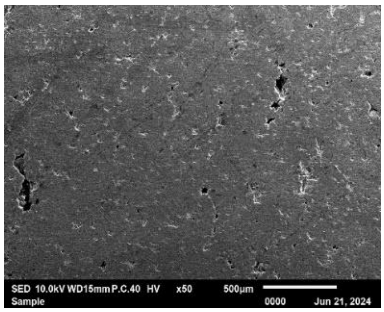

Fig. 8. sample 2

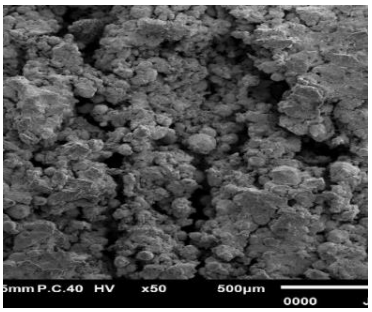

Fig. 9. sample 3

To further investigate the importance of infill density and holding hours during the debinding and sintering processes, regression analysis and Taguchi methods were applied to examine the Z-axis shrinkage. These analyses were conducted using Minitab 18 to identify the key factors and optimise the process parameters for improved material performance. The regression analysis in Table 3 was conducted to evaluate the impact of various factors on the shrinkage along the Z-axis of 3D printed samples. The analysis considered three main factors: infill density, holding hours for debinding, and holding hours for sintering.

Table 3. Regression analysis of Z axis shrinkage

Source	DF	Adj SS	Adj MS	F-Value	P-Value
Regression	3	63.286	21.095	13.00	0.008
Infill density	1	57.970	57.970	35.73	0.002
Holding hours for debinding	1	4.167	4.167	2.57	0.170
Holding hours for sintering	1	1.148	1.148	0.71	0.439
Error	5	8.112	1.622		
Total	8	71.397			

The infill density has a significant effect on the response variable, as indicated by its low P-value and high F-value. This factor explains a substantial portion of the variation. Holding hours for debinding and sintering, these factors do not have significant effects, as indicated by their higher P-values. The significant impact of infill density on shrinkage underscores its importance in the setup of 3D printing processes. Higher infill densities are likely to contribute to greater internal stresses during cooling, leading to more pronounced shrinkage. This factor's strong statistical significance suggests that controlling infill density can be a key strategy for minimising Z-axis shrinkage and achieving dimensional accuracy.

Table 4 is from Taguchi analyses. Infill density shows the highest delta value of 14.271, indicating that changes in infill density have the most substantial impact on Z-axis shrinkage. Holding Hours for Debinding exhibits the second highest impact on shrinkage, with a delta of 7.845. Among the factors tested, holding hours for sintering has the least impact on shrinkage, with a delta of 6.418. The shrinkage does not significantly vary with changes in sintering duration.

Table 4. Response Table for Signal to Noise Ratios z axis analysis, Smaller is better

Level	Infill density (%)	Holding hours for debinding (hours)	Holding hours for sintering (hours)
1	-17.585	-16.536	-16.280
2	-15.219	-8.692	-9.861
3	-3.314	-15.298	-14.299
Delta	14.271	7.845	6.418
Rank	1	2	3

The main effects plot for S/N ratios of Taguchi analysis in figure 10 highlights the influence of infill density, holding hours for debinding, and holding hours for sintering on the shrinkage along the Z-axis in 3D printed parts, with a focus on optimizing for "smaller is better" in terms of shrinkage.

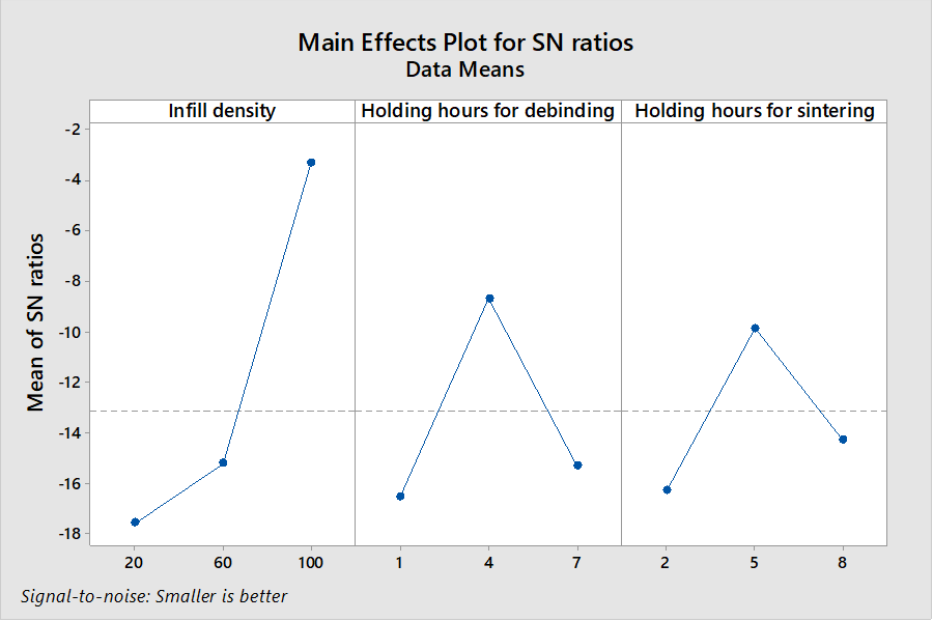

Fig. 10. Taguchi Analyses: Signal-Noise Ratio for Z axis shrinkage

Increasing the density of the infill material results in a stronger internal structure, which reduces the negative impact of thermal contraction and internal stresses that occur during the debinding and sintering processes. This more compact arrangement decreases the probability of distortion and contraction, which enhances the overall dimensional stability.

The plot reveals that holding hours for debinding have an optimal point at around 4 hours. Increasing the holding time beyond this point does not improve the SN ratio and may lead to increased shrinkage and other defects. This suggests that excessive debinding time can cause material degradation, affecting the final part quality. The plot demonstrates a nonlinear correlation between the duration of sintering and the signal-to-noise ratio. The most favourable duration for holding seems to be approximately 5 hours, at which point the signal-to-

noise ratio reaches its highest value. Deviation from the ideal period, whether shorter or longer, leads to less desirable effects.

Figures 11 and 12 show SEM analyses of sample 2 and sample 8. Sample 2, with 100% infill and 4 hours of debinding, still exhibits a layer gap at the z axis, indicating that the 100% infill has experienced less shrinkage. Sample 8, which had 20% infill and underwent 4 hours of debinding, demonstrates a significant reduction in the layer gap, although it remains somewhat visible.

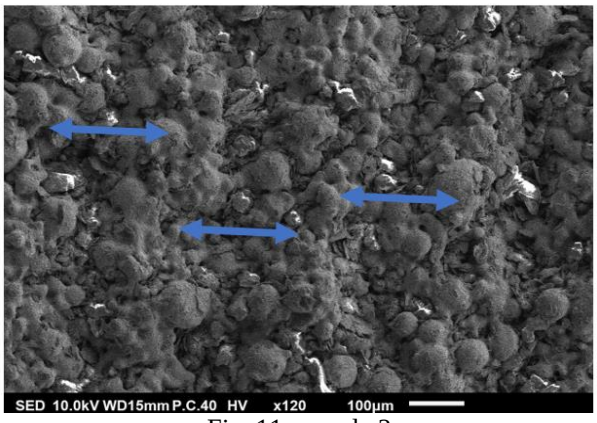

Fig. 11. sample 2

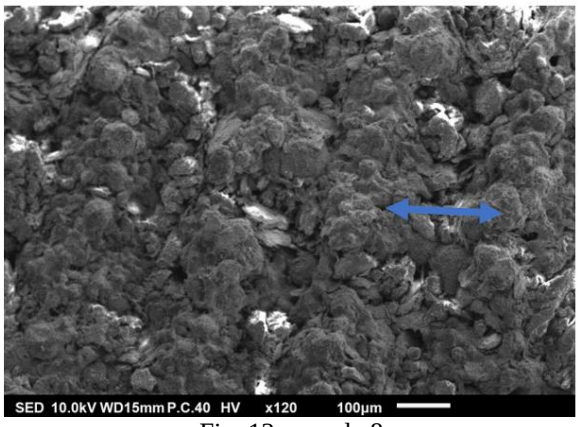

Fig. 12. sample 8

Regression analysis is employed to examine the shrinkage of the XY axis, with the aim of identifying the key parameters that have a substantial impact on the shrinkage behaviour. Regression analysis aids in determining the variables that exert the most significant influence on the shrinkage percentages. Table 5 presents the results of the regression analysis of variance, including the p-values for each parameter. The p-values will assist in assessing the statistical significance of the components under investigation, allowing us to focus on the parameters that significantly influence the XY axis' shrinkage.

Table 5. Regression analysis of xy axis shrinkage

Source	DF	Adj SS	Adj MS	F-Value	P-Value
Regression	3	0.005115	0.001705	8.96	0.019
Infill density	1	0.004507	0.004507	23.69	0.005
Holding hours for debinding	1	0.000114	0.000114	0.60	0.475
Holding hours for sintering	1	0.000494	0.000494	2.60	0.168
Error	5	0.000951	0.000190		
Total	8	0.006066			

Table 5 presents the variance regression analysis for the components that influence the XY axis shrinking. The table contains the degrees of freedom (DF), adjusted sums of squares (Adj SS), adjusted mean squares (Adj MS), F-values, and p-values for each source of variation. The regression model is statistically significant, as evidenced by a p-value of 0.019. This indicates that the model consistently forecasts the XY axis reduction. The infill density has a statistically significant effect at the 0.01 level, as indicated by a p-value of 0.005. These findings suggest that the density of infill material has a significant impact on the XY axis' shrinkage. Modifying this parameter is expected to cause substantial alterations in shrinkage. The p-value for holding hours during debinding is 0.475, indicating that this factor does not have a statistically significant impact. Changes in the duration of debinding do not significantly impact the shrinkage of the XY axis within the study's range. The p-value for the duration of holding hours during sintering is 0.168, which is above the standard significance level of 0.05. Our indicates that although there may be some impact, it does not have a statistically significant effect in our analysis.

Table 6 shows the response table for signal-to-noise (S/N) ratios with the criterion "smaller is better," focussing on the factors affecting XY axis shrinkage. The table includes the levels of each factor, their corresponding S/N ratios, delta values, and the rank of each factor's influence. The S/N ratio increases significantly from Level 1 to Level 3, with a delta of 3.90, indicating that infill density has the most substantial impact on shrinkage. In terms of influence, it ranks first. The S/N ratios for holding hours during debinding show minor variations across the levels, with a delta of 0.63. This indicates that this factor has the least influence on shrinkage, ranking it 3rd. The S/N ratios for holding hours during sintering show moderate variations, with a delta of 1.08, suggesting a moderate impact on shrinkage. This factor is ranked 2nd.

Table 6. Response Table for Signal to Noise Ratios xy axis analysis, Smaller is better

Level	Infill density (%)	Holding hours for debinding (hours)	Holding hours for sintering (hours)
1	16.44	17.78	18.63
2	16.98	17.68	17.58
3	20.35	18.31	17.55
Delta	3.90	0.63	1.08
Rank	1	3	2

The main effects plot for SN ratios in figure 13 shows how the mean signal-to-noise (SN) ratios change as the levels of each factor (infill density, holding hours for debinding, and holding hours for sintering) are changed. The "smaller is better" criterion indicates a preference for lower SN ratios. The infill density plot shows a significant increase in the mean SN ratio as the infill density increases from 20% to 100%. This steep upward trend suggests that infill density has a strong influence on the SN ratio, which is consistent with the high delta value (3.90) and the rank of 1 in Table 6. Higher infill densities lead to higher SN ratios, indicating a greater impact on shrinkage variability.

The plot for holding hours during debinding shows minimal variation across the different levels (1, 4, and 7 hours). This flat trend corresponds to a low delta value (0.63) and a rank of 3 in Table 6, indicating that this factor has the least influence on the SN ratio. The near-horizontal line confirms that changes in debinding time do not significantly impact shrinkage. The plot for holding hours during sintering shows moderate variation, with the SN ratio decreasing from level 1 (2 hours) to level 3 (8 hours). The delta value (1.08) and the rank of 2 in Table 6 reflect this moderate downward trend, suggesting a moderate influence on the SN ratio. The variation indicates that holding hours for sintering affect shrinkage, but to a lesser extent than infill density.

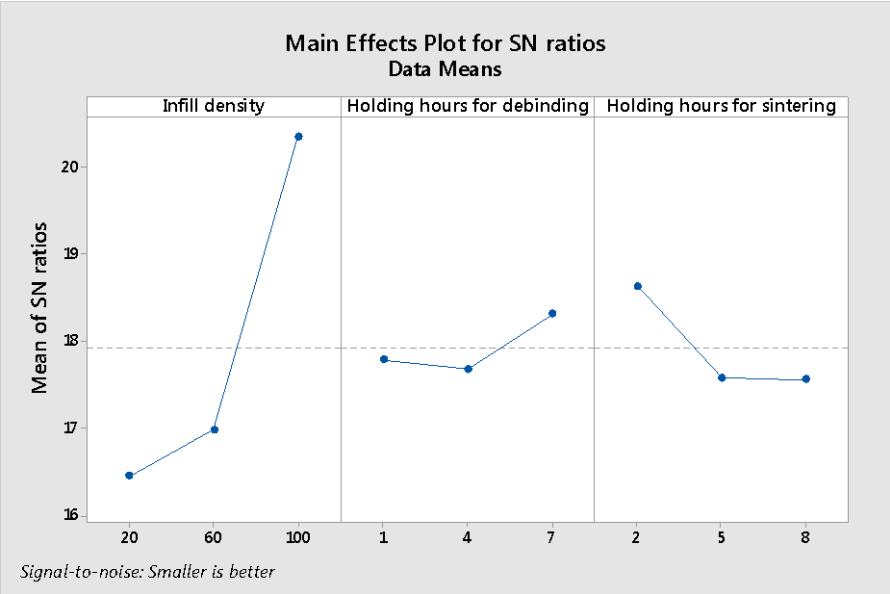

Fig. 13. Taguchi Analyses: Signal-Noise Ratio for xy axis shrinkage

Figures 14 and 15 are SEM analyses of sample 3 and sample 8. Sample 3 with 100% infill density and 2 hours of sintering have many larger holes compared to sample 8 with 100% infill and 2 hours of sintering. This hole shows that sample 8 has shrunk more than sample 3 causing the holes smaller.

The graph in figure 16 demonstrates substantial heterogeneity in the porosity across the samples. Sample 3 has the maximum porosity, measuring at 45.64%. This finding implies that the material may be more porous or that there are differences in the way the sample was prepared or the conditions it was subjected to. Based on their porosity levels, it can be inferred that samples 6, 7, and 8 exhibit the least number of pores, indicating that these materials or conditions resulted in the production of samples with the lowest porosity.

The regression analysis in Table 7 investigates the effects of infill density, holding hours for debinding, and holding hours for sintering on the porosity of 3D printed samples.

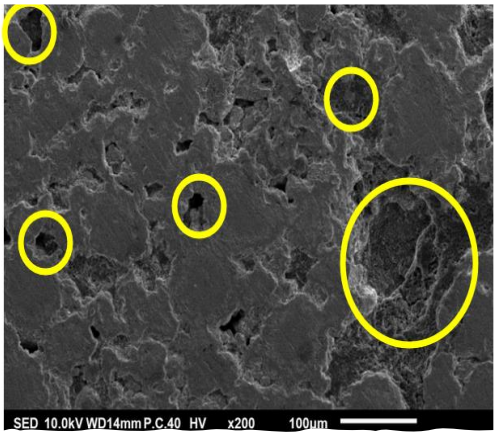

Fig. 14 sample 3

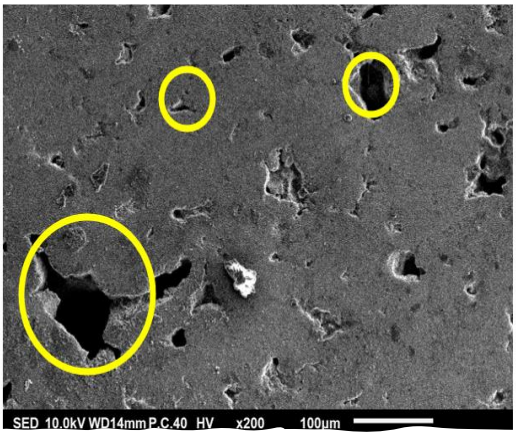

Fig. 15 sample 8

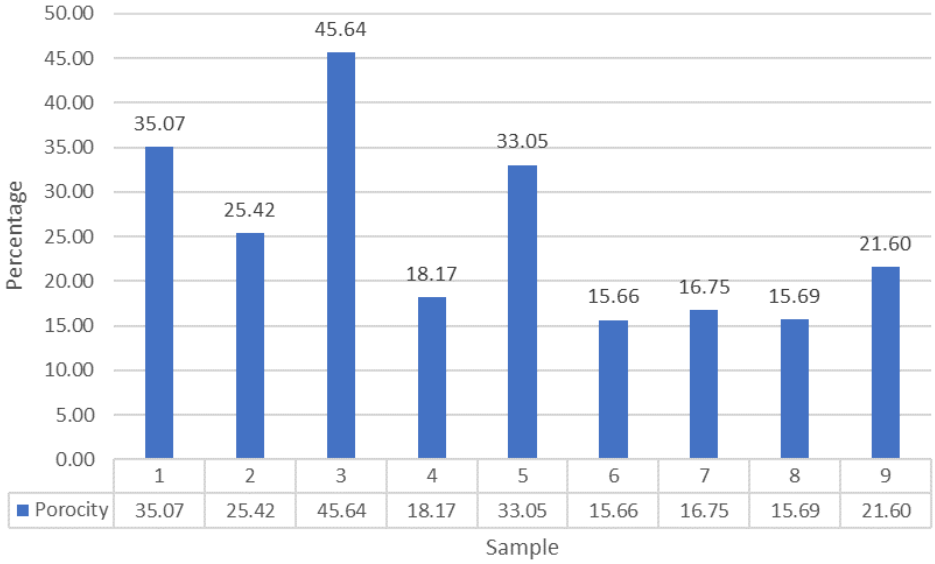

Fig. 16. Graph of percentage of porosity

Table 7. Regression analysis of porosity analysis

Source	DF	Adj SS	Adj MS	F-Value	P-Value
Regression	3	620.32	206.77	3.81	0.092
Infill density	1	452.23	452.23	8.33	0.034
Holding hours for debinding	1	27.73	27.73	0.51	0.507
Holding hours for sintering	1	140.36	140.36	2.58	0.169
Error	5	271.54	54.31		
Total	8	891.86			

The P-Value of infill density factor is 0.034. Shows that the infill density significantly affects porosity, with a low p-value indicating strong statistical significance. Holding hours for debinding have the P-Value of 0.507 indicate that do not significantly influence porosity, as shown by the high p-value. The result of holding hours for sintering have a non-significant effect on porosity, indicated by the p-value is 0.169.

The only factor with a significant impact on porosity, suggesting that higher or lower infill densities substantially affect the void spaces within the printed structure. This finding implies that manipulating infill density can be an effective method to control porosity, which is crucial for applications where material density and mechanical properties are important. Neither debinding nor sintering duration significantly affects porosity. This might indicate that once optimal levels for these parameters are reached, further adjustments do not contribute significantly to changes in porosity. Alternatively, the range of hours tested might not have been sufficient to detect a significant difference, suggesting a need for broader experimentation.

Table 8 presents the results from a Taguchi analysis examining the effects of infill density, holding hours for debinding, and holding hours for sintering on shrinkage in 3D printed samples, measured at three different levels for each factor.

Table 8. Response Table for Signal to Noise Ratios porosity analysis, Smaller is better

Level	Infill density	Holding hours for debinding	Holding hours for sintering
1	-25.03	-27.92	-29.35
2	-26.49	-27.47	-26.66
3	-30.73	-26.86	-26.24
Delta	5.7	1.07	3.12
Rank	1	3	2

Infill Density has the highest delta, indicating it has the most significant influence on shrinkage. The holding hours for debinding shows the least variation across levels with a very small delta, indicating that changes in debinding duration have a minimal effect on shrinkage. The minor differences suggest that once the binder is removed, the remaining material structure does not significantly contract or expand based on the time spent in this phase. Holding hours for Sintering, holds an intermediate rank and shows a moderate level of influence on shrinkage, with shrinkage decreasing slightly as sintering time increases. This may indicate that longer sintering times allow for a more gradual and controlled heat application, reducing the likelihood of rapid thermal changes that can cause material distortion or shrinkage.
The S/N ratios graph in figure 17 from the Taguchi analysis provides insights into how the levels of infill density, holding hours for debinding, and holding hours for sintering impact the shrinkage characteristics of 3D printed samples.

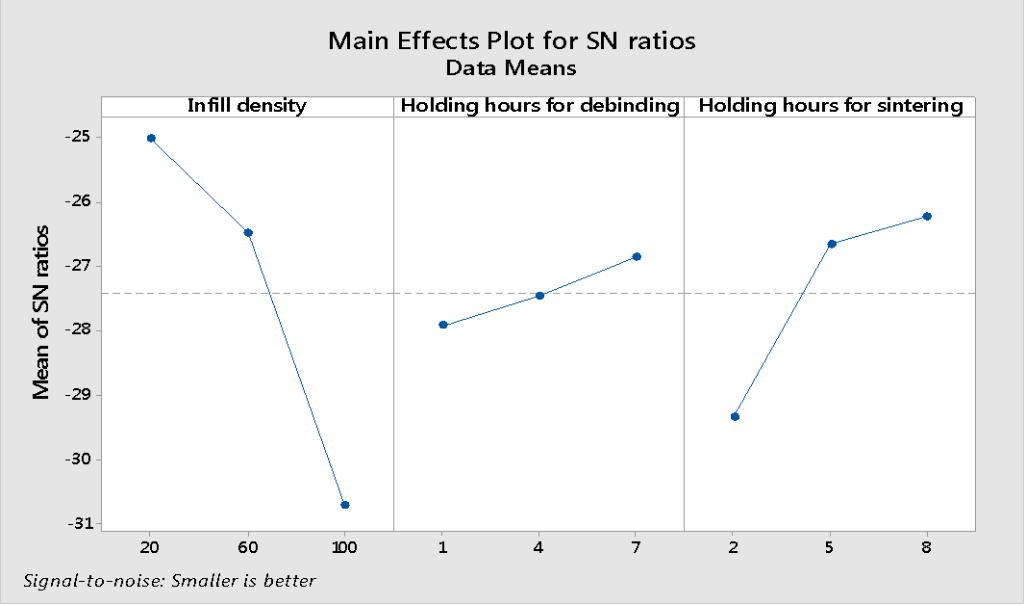

Fig. 17. Taguchi Analyses: Signal-Noise Ratio for porosity analysis

Infill Density shows a significant decrease in S/N ratios as infill density increases from 20% to 100%. This trend indicates a greater shrinkage at higher densities. Holding Hours for Debinding displays a slightly increasing trend in S/N ratios from 1 hour to 7 hours. The increase is moderate, suggesting that longer debinding times slightly improve the shrinkage outcomes, stabilizing the material. Holding Hours for Sintering indicates an increasing trend in S/N ratios as the sintering time is extended from 2 hours to 8 hours. This pattern suggests that longer sintering times are associated with reduced shrinkage, improving material integrity and dimensional stability.
Infill density is clear that downward trend in S/N ratios with increasing infill density underscores that higher densities exacerbate shrinkage. This could be due to increased material volume undergoing more significant thermal contraction and internal stress during cooling. Managing infill density is crucial for minimizing shrinkage, especially in applications where dimensional accuracy is critical. As for Holding Hours for Debinding and Sintering, the increase in S/N ratios with longer debinding and sintering times suggests that these processes, when

extended, help alleviate shrinkage. For debinding, this may allow more thorough removal of binders, reducing post-debinding contraction. For sintering, longer durations likely lead to a more uniform heat distribution and gradual cooling, which helps in minimizing thermal stresses that cause shrinkage. Figures 18 and 19 are Sample 1 with 100% and 8 hours of sintering have many holes compared to the sample 8 that have less holes. This shows that sample 8 has less porosity than sample 1.

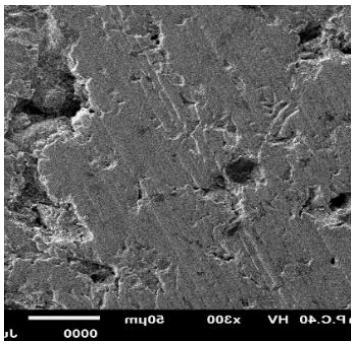

Fig. 18. sample 1

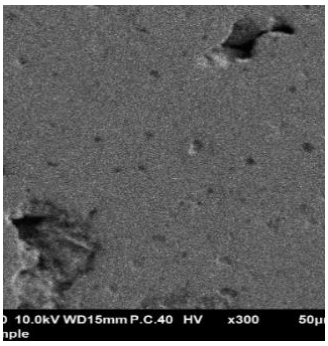

Fig. 19. sample 8

The Energy Dispersive X-ray (EDX) spectroscopy used to determine the complete removal of the binder. It provides a comprehensive breakdown of the material percentages in samples following the debinding and sintering procedures. Figure 20 shows the data obtained during the analysis.

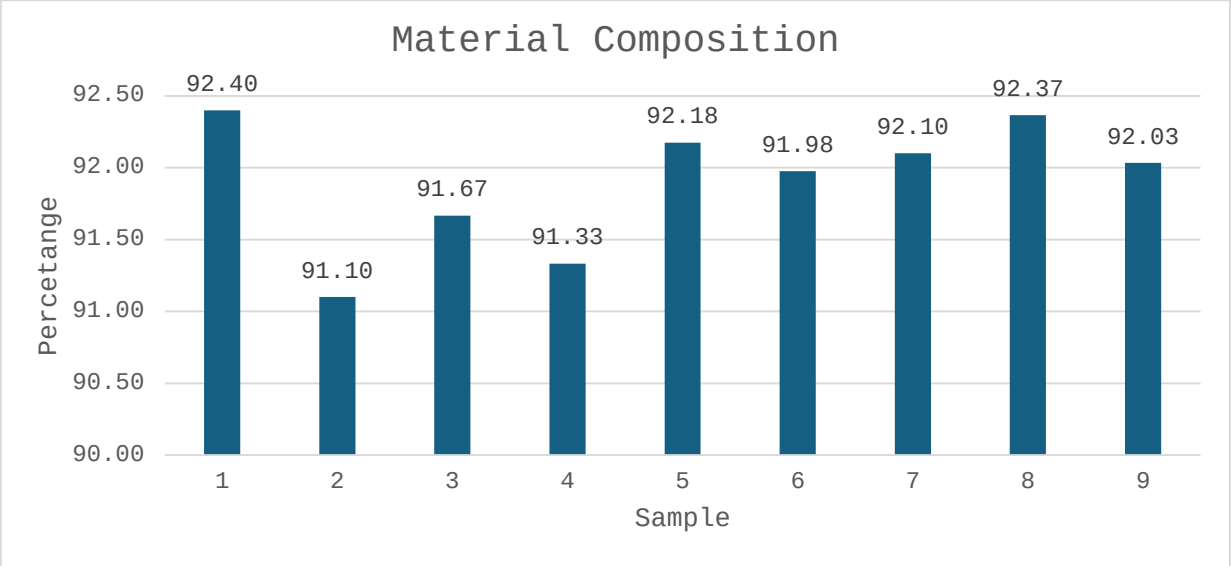

Fig. 20. Material composition Data

The graph displays little variation in material composition across the nine samples, all falling within the limited range of 91.10% to 92.40%. These findings indicate that the samples exhibit a high level of material uniformity with few deviations. The samples with the highest percentages, specifically Samples 1, 8, 5, and 7, may suggest the most optimal or intended material composition for the specific application under investigation. These values indicate a higher concentration of the main material component in the samples. The proportion of material composition in Sample 2 is the lowest. This could be because of a problem with the processing method or a change in the source material that caused the desired component to be less present.

Although there are minor differences, the collective composition of all samples consistently exceeds 91%, demonstrating a high degree of uniformity in material composition. The consistency of material qualities is critical for applications that require uniformity, such as manufacturing processes or quality control scenarios. In general, the data indicates that there is minimal variation in material composition among the samples, suggesting that the processes utilised for material processing or formulation are successful in keeping a constant composition.

Table 4.8 shows the regression analysis of the material composition to determine the impact of factors on samples. The results show that the p-value is not significant because it is above 0.05. The infill density and holding hours of debinding and sintering are not important in controlling the material composition. The factors are deemed insignificant, so no further analyses will be conducted.

Table 9 .Regression analysis of material composition analysis

Source	DF	Adj SS	Adj MS	F-Value	P-Value
Regression	3	0.49268	0.16423	0.40	0.758
Infill density	1	0.29630	0.29630	0.73	0.433
Holding hours for debinding	1	0.04279	0.04279	0.10	0.759
Holding hours for sintering	1	0.15360	0.15360	0.38	0.566
Error	5	2.03905	0.40781		
Total	8	2.53173			

The lack of variation in material composition in post-sintering is indicative of effective process control and material stability, which are essential for the reproducibility and reliability of 3D printed objects. This stability suggests that the debinding and sintering parameters were optimally chosen to prevent decomposition or oxidation of copper despite the high temperatures involved in sintering.
The debinding process at a temperature of 482°C is sufficient to remove 100% of the binder from the filament. Previous research shows that the melting temperature of PLA is between 170°C and 190°C [22]. Therefore, the post process will manage to remove the binder from the sample.

4. CONCLUSIONS

This study created metal products using fused deposition modelling (FDM) 3D printing with copper-PLA filament from Virtual Foundry. Various printing and post-processing factors were investigated to analyse shrinkage, porosity, and material composition, resulting in three main findings:
Infill density had a significant impact on z axis and xy axis shrinkage, with 100% infill density being the most effective in minimizing shrinkage while preserving dimensional integrity. It was discovered that maintaining specific time intervals throughout the debinding process and sintering does not significantly affect the shrinkage. Infill density influenced porosity, with 20% infill exhibiting the least porosity. Extended sintering times, especially at 8 hours, led to decreased porosity compared to shorter durations, with a little change observed between 5 and 8 hours.
The material composition was not affected by the manipulation of infill density, holding hours of debinding and sintering, demonstrating the method's capability to consistently maintain the material composition in metal product manufacturing. Yet, attaining optimal product quality continues to be a struggle.
No direct link was found between z-axis or x-axis shrinkage values and porosity levels. A future study could concentrate on improving post-processing methods, especially on perfecting the debinding process. Studying factors like heating rate and peak temperature in the debinding process could enhance product accuracy and quality.

Funding: This paper has received no external funding.
Conflicts of Interest: There is no conflict of interest.

REFERENCES

1. S. Wickramasinghe, T. Do, P. Tran, (2020), *FDM-Based 3D printing of polymer and associated composite: A review on mechanical properties, defects and treatments*, Polymers, 12(7), 1529, https://doi.org/10.3390/polym12071529.
2. G. A. Roberson, P. K. Sinha, (2022), *3D printing in orthodontics: A practical guide to the printer technology and selection*, Semin Orthod, 28(2), 100–106, doi: 10.1053/j.sodo.2022.10.006.
3. J. Schiltz et al., (20200, *Wear behavior of additive manufactured zirconia*, Elsevier B.V., pp. 821–827. doi: 10.1016/j.promfg.2020.05.119.
4. J. Huang, Q. Qin, J. Wang, (2020), *A review of stereolithography: Processes and systems*, Processes, 8(9), 1138, https://doi.org/10.3390/pr8091138
5. N. Naveed, (2020), *Investigate the effects of process parameters on material properties and microstructural changes of 3D printed specimens using Fused Deposition Modelling (FDM)*, Materials Technology, 36(5), 317-330.
6. V. Shanmugam et al., (2021), *The mechanical testing and performance analysis of polymer-fibre composites prepared through the additive manufacturing*, Polymer Testing, 93, 106925, doi: 10.1016/j.polymertesting.2020.106925.
7. ***Filament metal and ceramic 3D printing materials, Available: 10.1016/j.polymertesting.2020.106925/, Accessed: May 02, 2023.

8. A. Kulkarni, J. M. Pearce, (2023), *Patent Parasites: Non-Inventors Patenting Existing Open-Source Inventions in the 3-D Printing Technology Space*, Inventions, 8(6), 141; https://doi.org/10.3390/inventions8060141
9. C. Gloeckle, T. Konkol, O. Jacobs, W. Limberg, T. Ebel, U. A. Handge, (2020), *Processing of highly filled polymer–metal feedstocks for fused filament fabrication and the production of metallic implants*, Materials, 13(19), 1–16, doi: 10.3390/ma13194413.
10. M. Ortega Varela de Seijas, A. Bardenhagen, T. Rohr, E. Stoll, (2023), *A hybrid material extrusion device with local debinding and sintering*, Mater Today Commun, 36, doi: 10.1016/j.mtcomm.2023.106730.
11. C. Tosto, J. Tirillò, F. Sarasini, G. Cicala, (2021), *Hybrid metal/polymer filaments for fused filament fabrication (FFF) to print metal parts*, Applied Sciences, 11(4), doi: 10.3390/app11041444.
12. J. Khaliq, D. R. Gurrapu, F. Elfakhri, (2023), *Effects of Infill Line Multiplier and Patterns on Mechanical Properties of Lightweight and Resilient Hollow Section Products Manufactured Using Fused Filament Fabrication*, Polymers, 15(12), doi: 10.3390/polym15122585.
13. N. A. Sukindar et al., (2024), *Evaluation of the surface roughness and dimensional accuracy of low-cost 3D-printed parts made of PLA–aluminium*, Heliyon, 10(4), doi: 10.1016/j.heliyon.2024.e25508.
14. O. I. Ayeni, (2018), *Sintering and characterizations of 3d printed bronze metal filament*, available at: https://docs.lib.purdue.edu/dissertations/AAI30502043/.
15. E. Moritzer, C. L. Elsner, C. Schumacher, (2021), *Investigation of metal-polymer composites manufactured by fused deposition modeling with regard to process parameters*, Polym Compos, 42(11), 6065–6079, doi: 10.1002/pc.26285.
16. S. Bhandari et al., (2024), *Ultra-rapid debinding and sintering of additively manufactured ceramics by ultrafast high-temperature sintering*, J Eur Ceram Soc, 44(1), 328–340, doi: 10.1016/j.jeurceramsoc.2023.08.040.
17. T. Kurose et al., (2020), *Influence of the layer directions on the properties of 316l stainless steel parts fabricated through fused deposition of metals*, Materials, 13(11), doi: 10.3390/ma13112493.
18. C. Tosto, J. Tirillò, F. Sarasini, C. Sergi, G. Cicala, (2022), *Fused Deposition Modeling Parameter Optimization for Cost-Effective Metal Part Printing*, Polymers, 14(16), doi: 10.3390/polym14163264.
19. X. Wei, I. Behm, T. Winkler, S. Scharf, X. Li, R. Bähr, (2022), *Experimental Study on Metal Parts under Variable 3D Printing and Sintering Orientations Using Bronze/PLA Hybrid Filament Coupled with Fused Filament Fabrication*, Materials, 15(15), doi: 10.3390/ma15155333.
20. Nor Aiman Sukindar, Muhammad Afif Md Azhar, Nor Farah Huda Abd Halim, Shafie Kamaruddin, Mohd Hafis Sulaiman, (2020), *The Effects of Printing Parameters on The Surface Quality of Metal Composite by Using Fused Deposition Modeling*, Solid State Technology, 63(5), 866-874, available: www.solidstatetechnology.us
21. M. C. Vu, T. H. Jeong, J. B. Kim, W. K. Choi, D. H. Kim, S. R. Kim, (2021), *3D printing of copper particles and poly(methyl methacrylate) beads containing poly(lactic acid) composites for enhancing thermomechanical properties*, J Appl Polym Sci, 138(5), doi: 10.1002/app.49776.
22. N. G. Khouri, J. O. Bahú, C. Blanco-Llamero, P. Severino, V. O. C. Concha, E. B. Souto, (2024), *Polylactic acid (PLA): Properties, synthesis, and biomedical applications – A review of the literature*, Elsevier B.V. doi: 10.1016/j.molstruc.2024.138243.

Received: April 5th, 2024 / Accepted: December 15th, 2024 / Paper available online: December 20th, 2024